Commun Nonlinear Sci Numer Simulat 19 (2014) 3346–3361

Contents lists available at ScienceDirect

Commun Nonlinear Sci Numer Simulat

journal homepage: www.elsevier.com/locate/cnsns

Dynamics of landslide model with time delay and periodic parameter perturbations

Srđan Kostić [a,*], Nebojša Vasović [b], Igor Franović [c], Dragutin Jevremović [d], David Mitrinovic [e], Kristina Todorović [f]

[a] Department of Geology, University of Belgrade, Faculty of Mining and Geology, Đušina 7, 11000 Belgrade, Serbia
[b] Department of Applied Mathematics, University of Belgrade, Faculty of Mining and Geology, Đušina 7, 11000 Belgrade, Serbia
[c] Department of Theoretical Mechanics, Statistical Physics, and Electrodynamics, University of Belgrade, Faculty of Physics, Studentski Trg 12, 11000 Belgrade, Serbia
[d] Department of Geotechnics, University of Belgrade, Faculty of Mining and Geology, Đušina 7, 11000 Belgrade, Serbia
[e] Institute for the Development of Water Resources "Jaroslav Černi", Jaroslava Černog 80, 11226 Belgrade, Serbia
[f] Department of Physics and Mathematics, University of Belgrade, Faculty of Pharmacy, Vojvode Stepe 450, 11000 Belgrade, Serbia

ARTICLE INFO

Article history:
Received 11 October 2013
Received in revised form 24 January 2014
Accepted 10 February 2014
Available online 20 February 2014

Keywords:
Landslides
Time delay
Stress perturbation
Rate-and state-dependent friction law

ABSTRACT

In present paper, we analyze the dynamics of a single-block model on an inclined slope with Dieterich–Ruina friction law under the variation of two new introduced parameters: time delay T_d and initial shear stress μ. It is assumed that this phenomenological model qualitatively simulates the motion along the infinite creeping slope. The introduction of time delay is proposed to mimic the memory effect of the sliding surface and it is generally considered as a function of history of sliding. On the other hand, periodic perturbation of initial shear stress emulates external triggering effect of long-distant earthquakes or some non-natural vibration source. The effects of variation of a single observed parameter, T_d or μ, as well as their co-action, are estimated for three different sliding regimes: $\beta < 1$, $\beta = 1$ and $\beta > 1$, where β stands for the ratio of long-term to short-term stress changes. The results of standard local bifurcation analysis indicate the onset of complex dynamics for very low values of time delay. On the other side, numerical approach confirms an additional complexity that was not observed by local analysis, due to the possible effect of global bifurcations. The most complex dynamics is detected for $\beta < 1$, with a complete Ruelle–Takens–Newhouse route to chaos under the variation of T_d, or the co-action of both parameters T_d and μ. These results correspond well with the previous experimental observations on clay and siltstone with low clay fraction. In the same regime, the perturbation of only a single parameter, μ, renders the oscillatory motion of the block. Within the velocity-independent regime, $\beta = 1$, the inclusion and variation of T_d generates a transition to equilibrium state, whereas the small oscillations of μ induce oscillatory motion with decreasing amplitude. The co-action of both parameters, in the same regime, causes the decrease of block's velocity. As for $\beta > 1$, highly-frequent, limit-amplitude oscillations of initial stress give rise to oscillatory motion. Also for $\beta > 1$, in case of perturbing only the initial shear stress, with smaller amplitude, velocity of the block changes exponentially fast. If the time delay is introduced, besides the stress perturbation, within the same regime, the co-action of T_d ($T_d < 0.1$) and small oscillations of μ induce the onset of deterministic chaos.

* Corresponding author. Tel.: +381 113219107.
E-mail addresses: srdjan.kostic@rgf.bg.ac.rs (S. Kostić), nvasovic@rgf.bg.ac.rs (N. Vasović), igor.franovic@gmail.com (I. Franović), jevremovic@rgf.bg.ac.rs (D. Jevremović), davidmitrinovic@yahoo.com (D. Mitrinovic), kisi@pharmacy.bg.ac.rs (K. Todorović).

http://dx.doi.org/10.1016/j.cnsns.2014.02.012
1007-5704/

1. Introduction

Landslides constitute a major geologic hazard of strong concern in most parts of the world, posing a serious threat to highway, railway and residential areas. They commonly occur in slopes of different geological and structural setting, and can be triggered by various external factors, such as floods, earthquakes or volcanic eruptions [1]. In order to occur, forces acting on a slope must overcome the friction strength along a possible sliding surface. The traditional way to asses whether a slope is safe or not relies mainly on the use of factor of safety by assuming a limit equilibrium of the soil [2,3]. This analysis commonly uses a simple static Coulomb failure criterion, where shear strength depends on the cohesion c and the angle of internal friction φ [4]. Here, the constant solid friction coefficient is interpreted as an effective average friction coefficient. This failure criterion simply requires reaching a critical stress threshold τ when instability occurs [5]. However, this failure model alone does not explain the time-dependent nature of the failure threshold and it holds only for $V = 0$. This temporal dependence of friction along a rough sliding surface was firstly observed in rock mass, and it has a significant impact on the earthquake nucleation [6]. Apparently, real observations, as well as laboratory experiments, indicate temporal logarithmic increase of friction coefficient during the interseismic interval or quasistationary contact between the block and rough surface in the Burridge–Knopoff model [7]. This type of friction is well described by Dieterich–Ruina rate-and state-dependent friction law, which has been studied extensively for rock joints [8–12]. Besides these experiments for dry rock joints, Skempton [13] observed similar behavior of clays in the ring shear tests, for much slower sliding rate ($V < 0.01$ mm/min), comparing to the results obtained for Burridge–Knopoff model [8,14,15]. Following the results of Skempton [13], it is reasonable to assume that Dieterich–Ruina rate-and state dependent friction law, with logarithmic increase of friction coefficient during the quasistationary contact, also holds for the landslides. Indeed, Chau [16] suggested that Dieterich–Ruina friction law with one state variable can be used to model landslides that occur in natural infinite slope along a plane of weak surface, such as a persistent rock joint, a rock joint filled with wet gouge or soil or a soil interface. Some years later, further research conducted by Chau [17] showed that two state variables are often needed for a more complete description of the shear stress evolution with deformation, motivated by the experiments on quartzite [9], dolomite [18] and granite [12].

Triggering and propagation of shallow landslides is commonly modeled by using a discrete element method [19] or a molecular dynamics approach [20]. In this paper, following the suggestion of Chau [16] and Helmstetter et al. [1], we assume that the sliding process could be described by a single sliding block moving along the rough surface. In particular, we model a landslide as a block resting on an inclined slope forming an angle φ with respect to the horizontal [21–23]. This phenomenological model describes only the landslides with translational slope failures, which can be idealized by infinite slope assumptions like the Vaiont landslide or La Clapiere landslide [1]. Furthermore, we assume that a pre-existing weak plane exists within the slope, and that a landslide occurs as a consequence of the unstable slip of a creeping slope when it is subject to small external perturbation [22,24,25].

As for the nature of friction between the block and the rough surface, we suppose that it could be described by Dieterich–Ruina friction law, but with only one state variable. The effect of the other state variable, as well as the delayed increase in frictional strength, is modeled by introducing the time delay parameter T_d in friction term. This kind of analysis was already applied for the earthquake nucleation model in our previous research [26]. Another reason for inclusion of time delay in friction term is that the delayed increase of static friction coefficient is observed in laboratory experiments, as well as in the quiescent period of seismic stress drop during the recurrence interval [6]. By assuming the analogy between the landslide faults and tectonic faults [27–29], it is plausible that this feature is also inherent for the friction coefficient along the sliding surface. It has to be emphasized that our approach here differs from the research on spring-block Burridge–Knopoff model of earthquake nucleation, primarily because gravitational pull is considered instead of spring–slider system.

Besides the introduction of time delay, the second part of the analysis included the external triggering effect of earthquake, by assuming periodic sinusoidal perturbations of the initial shear stress s_0. The sinusoidal earthquake signal could correspond to long duration shear seismic wave [28,30], or it could be generated by non-natural sources such as vehicle traffic [28]. As far as the authors are aware, this analysis is new and the seismic impact on landslide dynamics has not been investigated in this way so far. However, similar analysis was conducted for some biological systems [31], where periodic

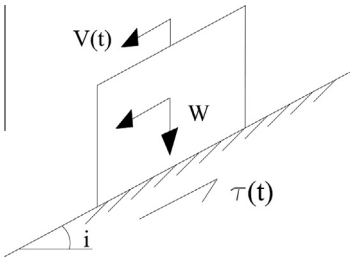

Fig. 1. The single-block model of landslide on an inclined slope with velocity $V(t)$ under gravitational pull.

parameter perturbation are attributed to various slow internal and external changes of the surrounding environment, basic variables and processes.

The paper consists of the following sections. In the first section, original model is described together with the corresponding Dieterich–Ruina rate-and state-dependent friction law. Here we also present results of the previous research and motivate our further analysis. In the second section, time delay parameter T_d is introduced and the dynamics of the system is analyzed numerically and by the means of standard local bifurcation analysis. In the third section we assume periodic perturbation of initial shear stress μ, and observe the changes in the landslide dynamics. In the fourth section, we analyze the co-action of both parameters T_d and μ. In the final section, we give discussion on the obtained results, together with the proposal for the future research.

2. Description of the original model and its derivatives

The aim of this paper is to provide a general framework which applies the one state variable friction law to landslide problems. To make the problem mathematically tractable, we only consider landslides which can be idealized by infinite slope assumptions (Fig. 1), as suggested in the work of Chau [16,17].

According to Chau [16], a motion of the single block on an inclined slope could be described by the system of three coupled nonlinear first-order differential equations:

$$\begin{aligned} \frac{dV}{dt} &= g\sin\alpha - \frac{\tau}{\rho h} \\ \frac{d\tau}{dt} &= \frac{d\theta}{dt} + \frac{A}{V}\frac{dV}{dt} \\ \frac{du}{dt} &= V \end{aligned} \tag{1}$$

where g is gravitational constant (9.81 m/s^2), α is the slope angle, ρ is the mass density, h is the thickness of the overlying soil, τ is the shear strength along the sliding surface, V and u are the velocity and displacement of the block, respectively, while A represents material constant, dependent on rock type, pressure, temperature and sliding velocity [32].

We model the shear strength along the sliding surface using a rate- and state-dependent friction law, which was originally developed to characterize laboratory observations of fault friction dependence on slip, time and sliding velocity [9]. In present paper, the choice of such friction model for sliding process was motivated by the results of laboratory analysis in the work of Skempton [13], which showed that this friction model is also valid for fluid-saturated clay and siltstone containing low clay fraction:

$$\begin{aligned} \tau &= \tau_0 + \theta + A\ln\left(\frac{V}{V_0}\right) \\ \frac{d\theta}{dt} &= -\frac{V}{L}\left[\theta + B\ln\left(\frac{V}{V_0}\right)\right] \end{aligned} \tag{2}$$

For $V = 0$, it is assumed that Coulomb's friction law applies: $\tau_0 = \mu\sigma$, where μ and σ are the frictional coefficient and the normal stress at the slip surface. In model (2) τ_0 represents the threshold shear stress at some reference sliding velocity V_0, B is an empirical constant, depending on the properties of soil, L is a characteristic slip distance comparable to a typical asperity length (characteristic decay length scale), while θ denotes the time-dependent state variable, which is a function of the history of sliding [33]. State variable θ represents an evolving time scale, as a delayed reaction of friction to instantaneous changes in velocity [34]. In the static case, $\theta = t$, and Dieterich [8] suggested that θ can be interpreted as the average age of contacts, i.e. the average elapsed time since the contacts were first formed. In present case, this variable is introduced to characterize the current mechanical state of the slip surface, and, in general, θ remains constant for the steady state, but evolves for unsteady slip [16].

Following the idea of Chau [16], the model of infinite slope evolution could be expressed in the subsequent dimensionless form:

$$\begin{aligned} \frac{ds}{dT} &= -\lambda e^{v}[s - s_0 - (1-\beta)v] + \frac{e^{-V}}{\kappa}(\gamma - s) \\ \frac{dv}{dT} &= \frac{e^{-v}}{\kappa}(\gamma - s) \\ \frac{d\delta}{dT} &= e^{v} \end{aligned} \tag{3}$$

where $s = \tau/A$ (dimensionless stress), $v = ln(V/V_0)$ (dimensionless velocity), $\delta = u/h$ (dimensionless displacement), $T = V_0 t/h$ (dimensionless time), $s_0 = \tau_0/A$, $\kappa = \rho V_0^2/A$, $\gamma = \rho ghsin\alpha/A$, $\beta = B/A$ and $\lambda = h/L$.

Equilibrium point for the system (3) is obtained by assuming that $ds/dT = dv/dT = 0$, while $d\delta/dT = const.$ Hence, the parameter values at the equilibrium point must satisfy the following conditions:

$$\begin{aligned} s &= \gamma \\ v &= \frac{\gamma - s_0}{1-\beta} \\ \delta &= e^v T \end{aligned} \tag{4}$$

In present analysis, the initial conditions (s, v, δ) are set near the equilibrium point.

The dynamics of this original model [16] for various range of parameter values shows two different stability regimes depending on parameter β, as the control parameter whose values determine the onset of bifurcations. For $\beta < 1$, which corresponds to velocity strengthening behavior, the motion of the block along the slope is so slow, that it could be approximated by the steady state of the block. All the solutions approach the improper node as $t \to \infty$. Similarly, for $\beta = 1$, the block moves along the slope with constant velocity, whose magnitude rises with the change of parameter s_0 in the range $[0, 1]$. According to Chau [16] all trajectories of the system (3) in this regime converge to neutrally stable equilibrium point. On the other hand, for $\beta > 1$, which represents velocity weakening friction law, the motion becomes unstable in a way that velocity of the block increases very fast and for a certain time interval, it suddenly diverges to infinity. In present paper, in contrast to Chau [16], we neglect the negative values of the block velocity, which appears for $s_0 > 1$. This indicates the motion of the block in opposite direction, which is not possible for natural sliding process, except for periodic perturbations due to earthquake triggering. Also, in contrast to Chau [16] we consider only the positive values of parameter β, since long-term or short-term stress changes cannot take negative values. Parameters λ, κ, β and γ have positive values.

3. Extended model with time delay

In the first phase of the research, we incorporate time delay in model (3) in the following way:

$$\begin{aligned} \frac{ds}{dT} &= -\lambda e^V [s(T - T_d) - s_0 - (1-\beta)v] + \frac{e^{-v}}{\kappa}(\gamma - s) \\ \frac{dv}{dT} &= \frac{e^{-v}}{\kappa}(\gamma - s) \\ \frac{d\delta}{dT} &= e^v \end{aligned} \tag{5}$$

where meaning of all terms is the same as in (3). In this way, we also model the influence of the second state variable, introduced previously in the work of Chau [17]. Apparently, the results of previous research showed that for the two-state variable friction law bifurcation occurs when the imaginary axis is crossed, as a dividing line of stable region and unstable region (Hopf bifurcation) [17].

The introduced time delay in dimensionless shear stress term emphasizes the delayed response of the friction (along the slip surface) to the sudden increase of sliding velocity. Such an abrupt velocity change is commonly caused by the effect of rainfalls, which is usually considered as the main triggering factor of slope instability. This assumption corresponds well with the results of laboratory test on fluid-saturated clay with low sliding rates, performed by Skempton [13], which clearly show the jump in shear stress before it decreases to the steady state value. Moreover, similar assumption has already been made in the case of a spring-block model of earthquake nucleation with much higher sliding rates [26], and it lead to new dynamical features. However, direct comparison of the present analysis with the previous researches on earthquake nucleation process cannot be made, since the present non-linear system is formulated by considering gravitational pull instead of spring–slider system, despite the fact that the same Dieterich–Ruina friction law is used.

3.1. Local stability and bifurcations of the stationary solution

The system (5) has only one stationary solution, namely $(s, v) = (1, 0)$, according to (4), for the following parameter values: $s_0 = \gamma = 1.0$, $\lambda = 1.5$, and $\kappa = 2.0$. We shall proceed in a standard way to determine and analyze the characteristic equation of (5) around a stationary solution $(1, 0)$.

Linearization of the system (5) and substitution $s = Ae^{\Delta T}$, $v = Be^{\Delta T}$ and $s(T - T_d) = Ae^{\Delta(T - Td)}$ results in a system of algebraic equations for the constants A and B. This system has a nontrivial solution if the Jacobian matrix satisfies the following condition:

$$\begin{vmatrix} -\frac{1}{\kappa} - \lambda e^{-\Delta T_d} - \Delta & \lambda(1-\beta) \\ -\frac{1}{\kappa} & -\Delta \end{vmatrix} = 0 \tag{6}$$

In other words, the characteristic equation of the system (5) must fulfill the following constraint:

$$\Delta^2 + \Delta\left(\frac{1}{\kappa} + \lambda e^{-\Delta T_d}\right) + \frac{\lambda}{\kappa}(1-\beta) = 0 \tag{7}$$

By substituting $\Delta = i\omega$ in (7), we obtain:

$$\frac{\omega^2 - \frac{\lambda}{\kappa}(1-\beta) - i\omega\frac{1}{\kappa}}{i\omega\lambda} = (\cos\omega T_d - i\sin\omega T_d) \tag{8}$$

The resulting two equations for the real and imaginary part of (8) after squaring and adding give an equation for the parameter β in terms of the other parameter ω, and vice versa, and after division, an equation for T_d in terms of the parameters β and ω. In this way, one obtains parametric representations of the relations between T_d and the parameters, which correspond to the bifurcation values $\Delta = i\omega$. The general form of such relations is illustrated by the following formula for β as a function of ω:

$$\beta_{1,2} = \frac{1}{2}\left[-\frac{8}{3}\omega^2 + 2 \pm \frac{8\sqrt{2}}{3}\omega\right] \tag{9}$$

On the other hand, for ω as a function of β:

$$\omega_{1,2}^2 = \frac{(14-6\beta) \pm 4\sqrt{2(5-3\beta)}}{8} \tag{10}$$

and for T_d as a function of β and ω:

$$T_d = \frac{1}{\omega}\left[arctg\left(\frac{2\left[\frac{3}{4}(1-\beta) - \omega^2\right]}{\omega}\right) + k\pi\right] \tag{11}$$

where k is any nonnegative integer such that $T_{dk} \geqslant 0$.

Though the very form of the solution adopted for the characteristic equation is indicative of Hopf bifurcations, the rigorous proof of this claim is rather lengthy to convey [35–37]. Here it suffices to say that the above parametric equations for β, ω and T_d coincide with the Hopf bifurcation curves illustrated in Fig. 2 for the fixed parameter values $s_0 = \gamma = 1.0$, $\lambda = 1.5$, and $\kappa = 2.0$.

Reading from Fig. 2, one learns that only by increasing the time-lag T_d, e.g. by setting $T_d = 0.5$, $T_d = 2$, $T_d = 7$ and $T_d = 10$, and by slightly changing the other parameter values, the block dynamics changes from the fixed point, over the limit cycle oscillation (first Hopf bifurcation) and torus (second Hopf bifurcation) to chaos. In particular, the system exhibits quasiperiodic (Ruelle–Takens–Newhouse) route to chaos [38,39]. Corresponding time series and phase portraits for points *a*, *b*, *c* and *d* in Fig. 2, are shown in Fig. 3. Broadband noise in Fourier power spectrum (Fig. 4) confirms the onset of deterministic chaos.

3.2. Numerical approach

In spite of the favorable results of the previous analysis indicating the onset of complex dynamics under the variation of the introduced time delay, we stress that the local stability analysis naturally does not capture the existence of global bifurcations. This is why we extended the analysis by numerically integrating model (5) near the equilibrium point (4). Regarding the fashion in which the delay-differential equations are numerically solved, the initial function is selected such that it is values within the interval $[-T_d, 0]$ are set by the first equation in (5) with $\lambda = 0$. In all the examined cases we adopt Runge–Kutta fourth order numerical integration method, due to simplicity and low computational cost, with the remark that qualitatively the same results could be obtained using an implicit integration scheme (e.g. backward differentiation formula), primarily intended for solving complex systems, as the one analyzed in this case. At each instance, the parameters

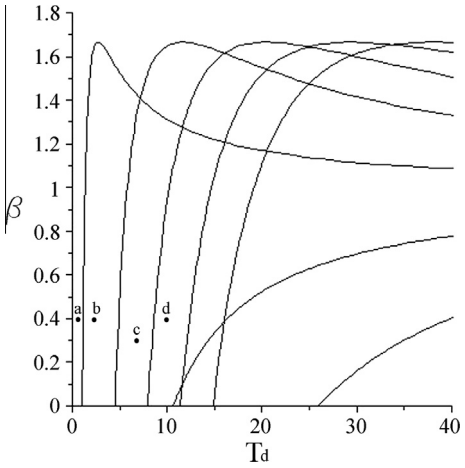

Fig. 2. Hopf bifurcation curves $T_d(\beta)$, for the fixed values of parameters $s_0 = \gamma = 1.0$, $\lambda = 1.5$, and $\kappa = 2.0$. The appropriate time series and the phase diagrams corresponding to points *a*, *b*, *c* and *d* are shown in Fig. 3.

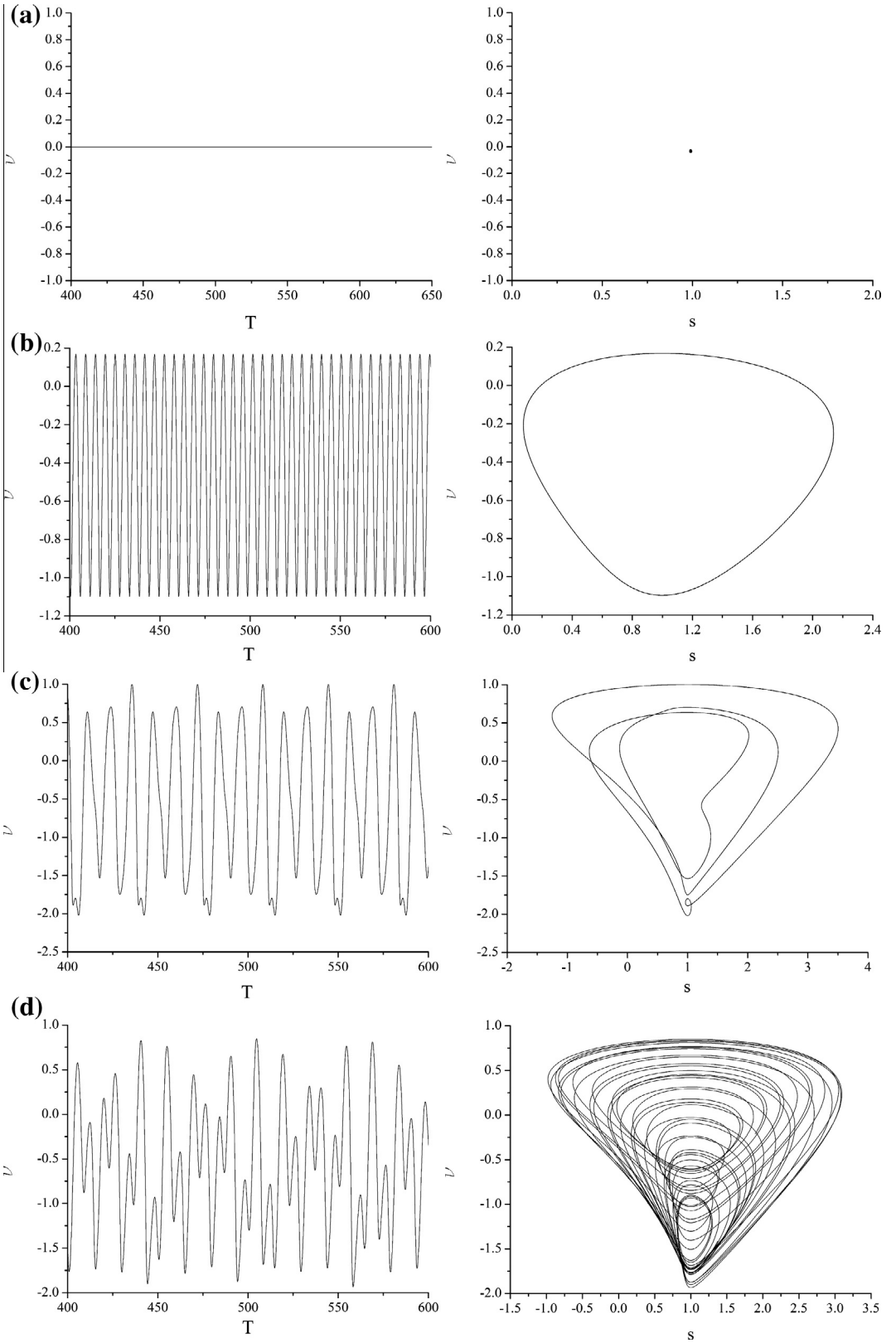

Fig. 3. Temporal evolution of variable V and the corresponding phase portraits for: (a) $T_d = 0.5$, $\beta = 0.4$, (equilibrium state); (b) $T_d = 2$, $\beta = 0.4$ (periodic motion); (c) $T_d = 7$, $\beta = 0.3$ (quasiperiodic motion); (d) $T_d = 10$, $\beta = 0.4$ (deterministic chaos). In all the examined cases, other parameter values are as in Fig. 2.

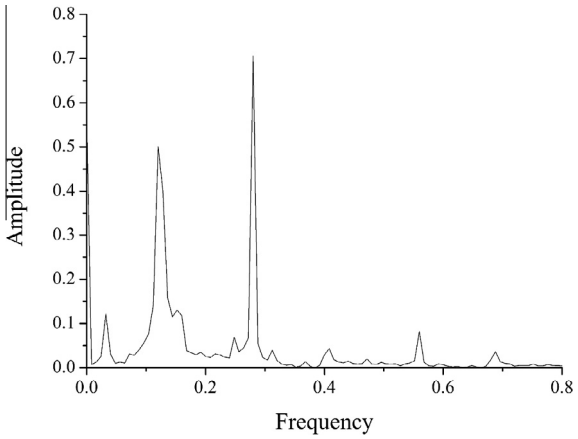

Fig. 4. Broadband noise in Fourier power spectrum indicates the chaotic behavior of the system. The parameter values are identical to those in Fig. 3(d).

held constant are awarded values near the equilibrium point. The dynamics of the block for $\beta < 1$ and for T_d in range [0.1–10] is shown in Fig. 5.

If we compare Figs. 2 and 5, it is clear that numerical approach indicates much complex behavior, with small areas of quasiperiodic and chaotic motion, which imply the existence of global bifurcations, which will not be analyzed in present paper.

The scenario of deterministic chaos was further confirmed by calculation of the Fourier power spectrum for oscillations, torus and chaotic orbits (Figs. 6 and 7a). The single peak in power spectrum in Fig. 6(a) indicates the oscillatory behavior of the system under study, while the quasiperiodic behavior (torus) is verified by the second peak in Fig. 6(b). The broadband noise in Fourier power spectrum (Fig. 7a) and positive value of maximal Lyapunov exponent, calculated by method of Wolf et al. [40] indicate that the attractor is strange (Fig. 7b).

In Fig. 8, the maximal Lyapunov exponent is calculated using the method of Rosenstein et al. [41]. One could note that the obtained values of $\lambda_{\max}$ by using the Wolf's (Fig. 7b) and Rosenstein's method (Fig. 8) are of the same order of magnitude.

For $\beta = 1$, system under study shows no complex dynamics under the increase of the included time delay. Apparently, for a first few values of time delay, the velocity of the block decreases in comparison to the original model, exhibiting finally a transition to equilibrium state. Further increase of time delay induce negative constant velocity of the block, meaning that block moves upwards, which is not physically possible, and this case is neglected in our analysis (Fig. 9). In other words, in

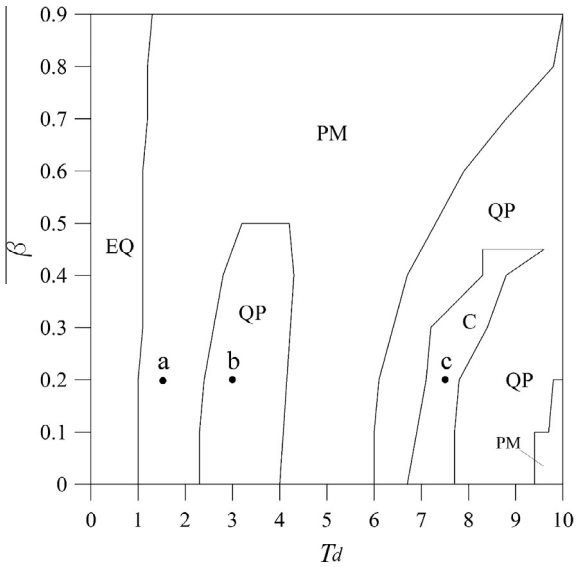

Fig. 5. Parameter domains (T_d, β), admitting equilibrium state (EQ), periodic (PM) and quasiperiodic motion (QP) and deterministic chaos (C). Diagram is constructed numerically, for the step size equal 0.1 for both T_d and β. Other parameter values are: $s_0 = 1.0$, $\lambda = 1.5$, $\kappa = 2.0$ and $\gamma = 1.0$. Corresponding power spectra for points *a*, *b* and *c* are shown in Fig. 6, while the largest Lyapunov exponent is calculated for point *c* in Fig. 7.

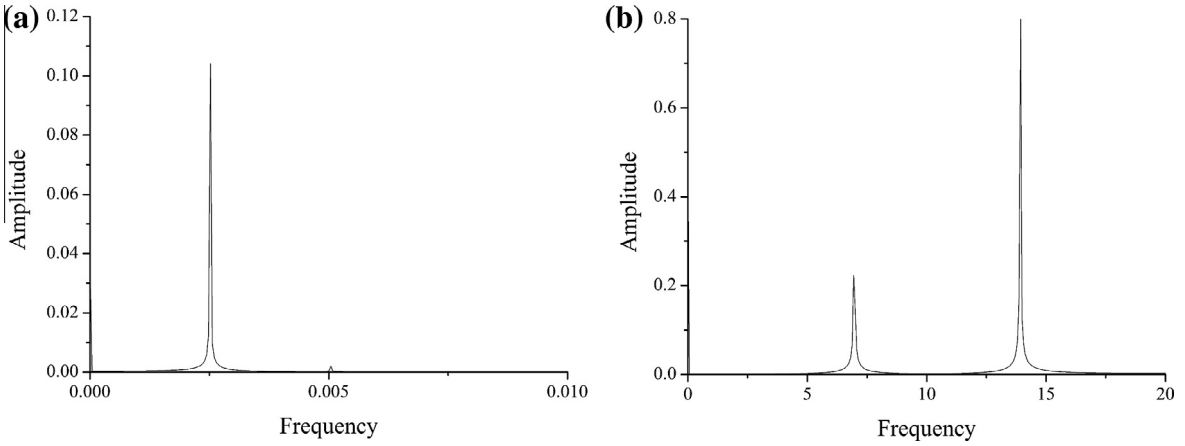

Fig. 6. (a) Single peak in power spectrum indicates the oscillatory behavior of the model for $T_d = 1.5$, $\beta = 0.2$ (point a in Fig. 5) (b) two peaks in power spectrum imply the appearance of torus for $T_d = 3$, $\beta = 0.2$ (point b in Fig. 5). In all the examined cases, other parameter values are as in Fig. 5.

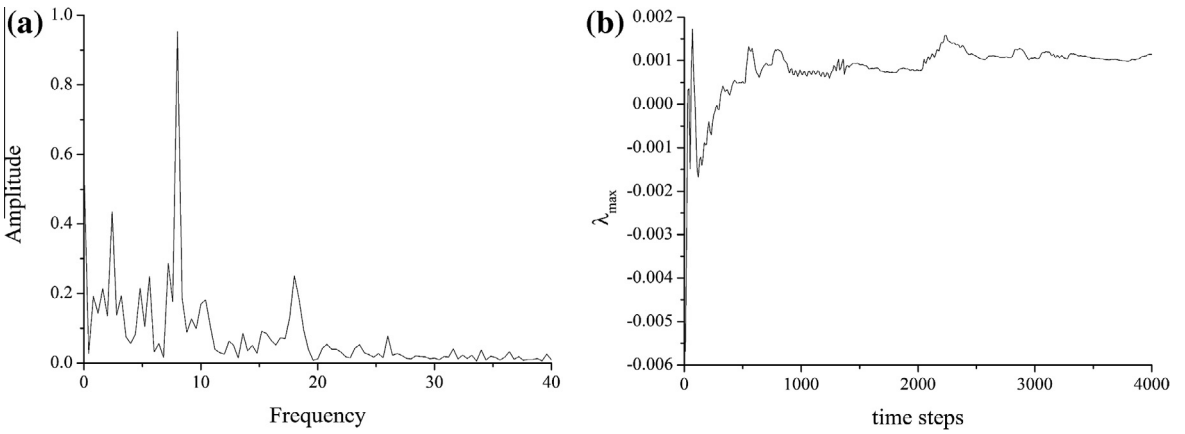

Fig. 7. (a) The broadband noise in Fourier power spectrum indicates the chaotic behavior of the system for $T_d = 7.5$, $\beta = 0.2$ (point c in Fig. 5); (b) maximal Lyapunov exponent converges well to $\lambda_{max} = 0.0011$, indicating the presence of deterministic chaos. Other parameter values are as in Fig. 5.

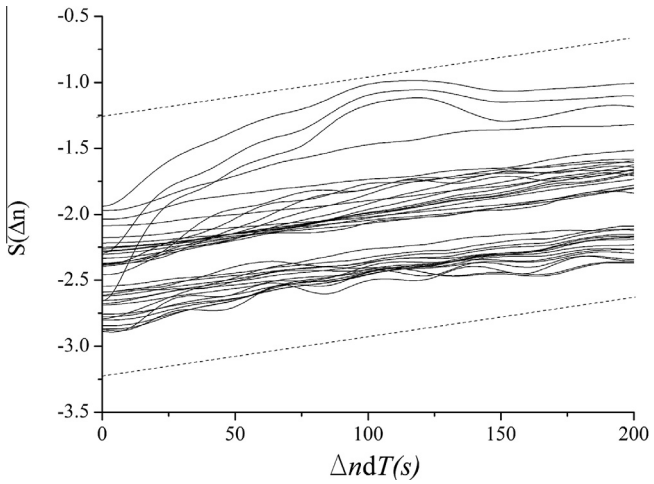

Fig. 8. Calculation of maximal Lyapunov exponent for the time series in Fig. 4 (4). The method of Rosenstein et al. [41], implies $\lambda_{max} \approx 0.003$. Effective expansion rate $S(\Delta n)$ represents the average of the logarithm of $D_i(\Delta n)$, defined as the average distance of all nearby trajectories to the reference trajectory as a function of the relative time Δn. The slope of dashed lines indicating the predominant slope of $S(\Delta n)$ in dependence on ΔndT presents a robust estimate for the maximal Lyapunov exponent. The results are determined for 1000 reference points and neighboring distance $\varepsilon = 0.15–0.30$. The obtained value of maximal Lyapunov exponent is of the same order of magnitude, as in Fig. 7(b).

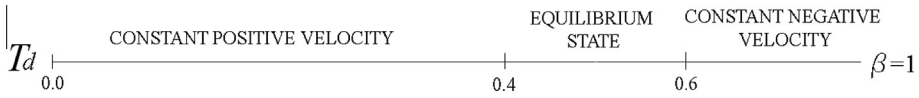

Fig. 9. Bifurcations of the system (5) under variation of parameter T_d, for $\beta = 1.0$. At each instance, the parameters held constant are awarded values near the equilibrium point: $s_0 = 1.0$, $\lambda = 1.5$, $\kappa = 2.0$, and $\gamma = 1.0$.

the case of $\beta = 1$, introduction of time delay suppresses the motion, leading eventually to equilibrium state of the block. This type of dynamics differs from the previous case, for $\beta < 1$, where the inclusion of T_d generated more complex behavior.

For $\beta > 1$, introduced time delay renders the system (5) extremely stiff in the plausible parameter domains, meaning that an exceedingly small iteration step ($<10^{-5}$) is required to carry out the numerical integration. However, the results of the analysis for $\beta = 1.1$ and $T_d = 0.1$, indicate the chaotic behavior of the model under study (Fig. 10), which is confirmed by continuous broadband noise in the power spectrum (Fig. 11a) and by positive value of the largest Lyapunov exponent (Figs. 11b and 12).

However, it should be emphasized that, even though the maximal Lyapunov exponent converged well to positive values in Figs. 7(b) and 11(b), the standard procedure of Wolf et al. [40] has to be complemented by performing additional averaging over a set of different initial conditions (Fig. 13), since delay-differential equation (5) represents infinite-dimensional system. It is clear that in all the examined cases, maximal Lyapunov exponent converges to positive value of the same order of magnitude as in Figs. 11(b) and 12.

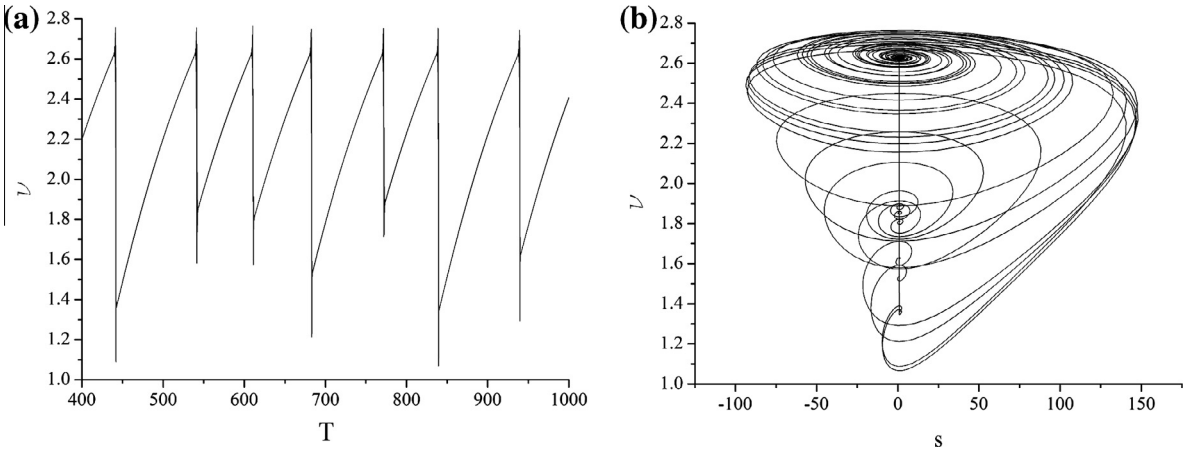

Fig. 10. (a) Time series $v(T)$ and (b) phase portrait for $\beta = 1.1$ and $T_d = 0.1$. Other parameter values are: $s_0 = 1.0$, $\lambda = 1.5$, $k = 2.0$, and $\gamma = 1.0$.

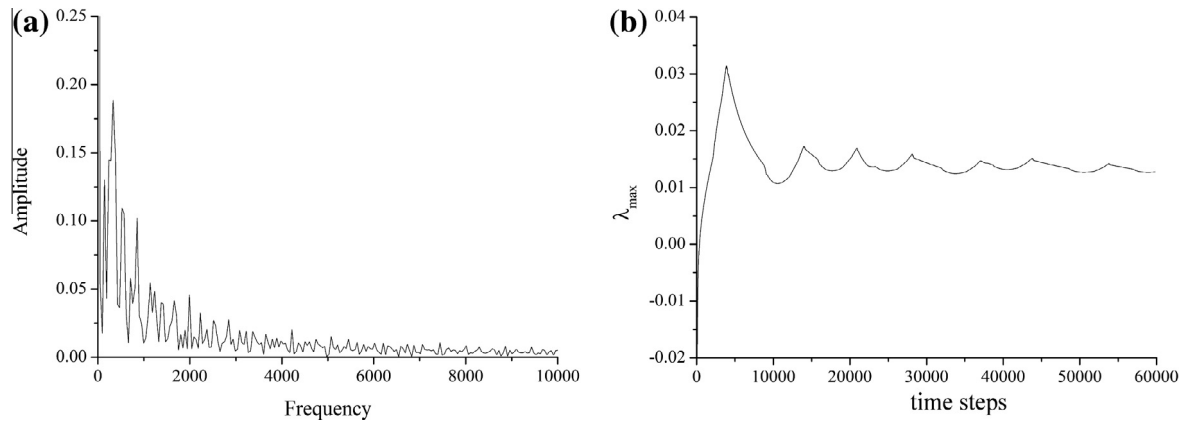

Fig. 11. (a) Continuous broadband noise in Fourier power spectrum confirms chaotic motion of block. (b) Maximal Lyapunov exponent converges well to positive value, $\lambda_{max} = 0.013$.

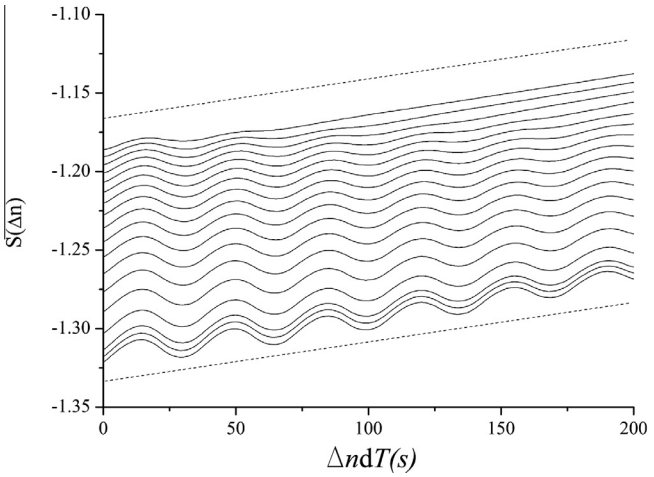

Fig. 12. Calculation of maximal Lyapunov exponent for the time series in Fig. 10(a). The method of Rosenstein et al. [41], implies $\lambda_{max} \approx 0.014$. The results are determined for 100 reference points and neighboring distance $\varepsilon = 0.5–1$. The obtained value of maximal Lyapunov exponent is of the same order of magnitude, as in Fig. 11(b).

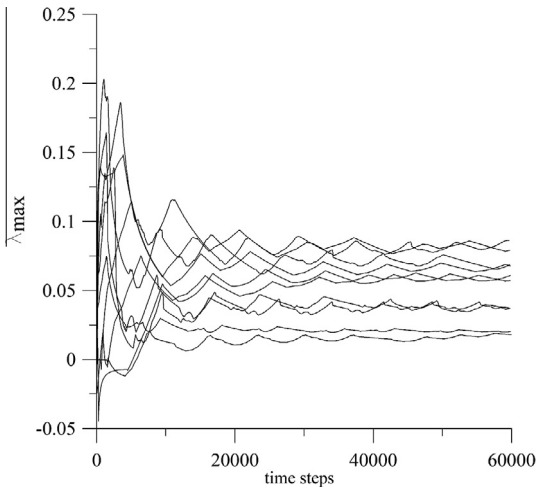

Fig. 13. Calculation of maximal Lyapunov exponent by performing additional averaging over a set of different initial conditions, whereby s_0, v_0 and δ_0 belong to the respective ranges $s_0 \in [0, 1]$, $v_0 \in [0, 0.5]$, $\delta_0 \in [0, 1]$. The results have been obtained by the method of Wolf et al. [41]. Maximal Lyapunov exponents converge well to positive values of the order 10^{-2}, the same as in Fig. 11(b). Note that time t is expressed in the units of iteration steps.

4. Extended model with stress perturbation

In the second phase of the analysis, we modified the original model (3) by assuming periodic perturbations of the initial shear stress s_0 due to external earthquake triggering effect:

$$\mu(T) = s_0 + \delta_s \sin(\omega_s T) \tag{12}$$

such that δ_s, and ω_s represent the constant oscillation amplitude and the angular frequency, respectively. The former satisfy the constraint $\delta_s \leqslant s_0$, which ensures the model's consistency as it confines each perturbation term to an appropriate range of values. In that way, system (3) becomes nonautonomous.

For $\beta < 1$, by perturbing only the shear stress μ, while the other parameters are held constant for the initally creeping slope (equilibrium state), block exhibits oscillatory behavior. This kind of motion is observed for any frequency value (ω_s) in the range [0.1–2.0]. It is in contrast to the original model, where only the constant positive velocity of the block is observed.

For $\beta = 1$, also by assuming limit amplitude oscillations of shear stress μ, the velocity of the block takes constant negative values, meaning that block moves upward, in opposite direction, which is physically impossible. Hence, this case is neglected in our analysis.

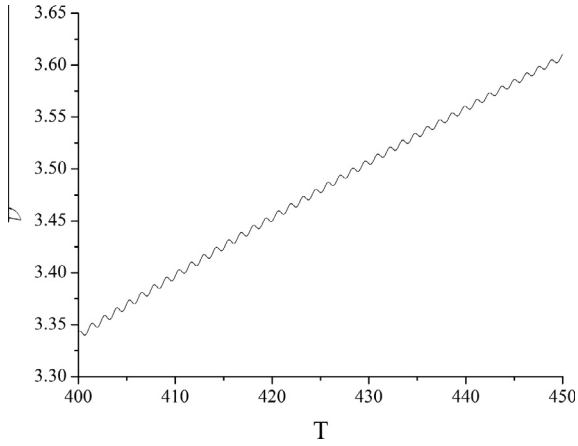

Fig. 14. Time series $v(T)$ for $\beta = 1.1$, and for oscillation amplitude $\delta_s = 1.0$ and frequency $\omega_s = 5.0$. At each instance, other parameters held constant are awarded values near the equilibrium point: $s_0 = 1.0$, $\lambda = 1.5$, $\kappa = 2.0$, and $\gamma = 1.0$.

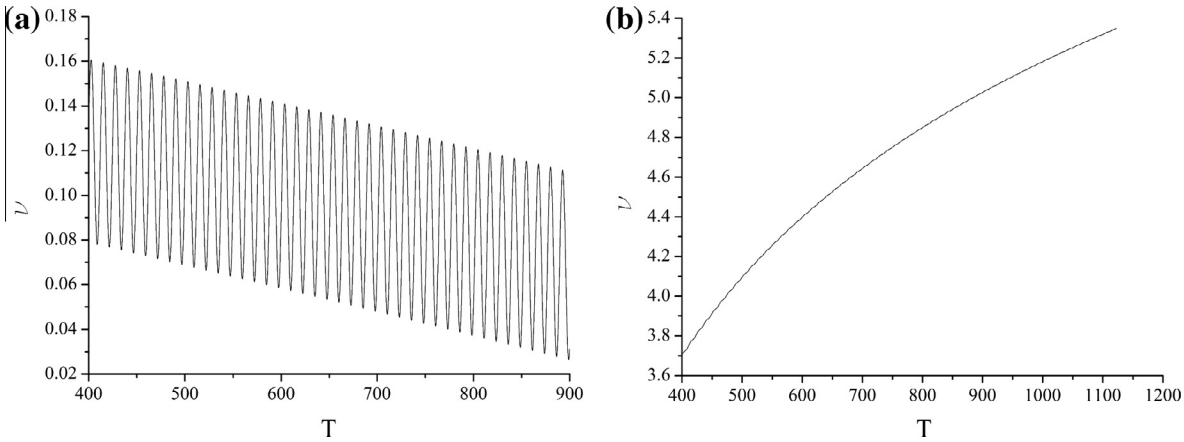

Fig. 15. (a) Time series $v(T)$ for $\beta = 1$, under the variation of parameter μ, with $\delta_s = 0.06$ and $\omega_s = 0.5$; (b) time series $v(T)$ for $\beta = 1.1$, and for oscillation amplitude $\delta_s = 0.2$ and frequency $\omega_s = 0.5$. At each instance, other parameters held constant are awarded values near the equilibrium point: $s_0 = 1.0$, $\lambda = 1.5$, $\kappa = 2.0$, and $\gamma = 1.0$.

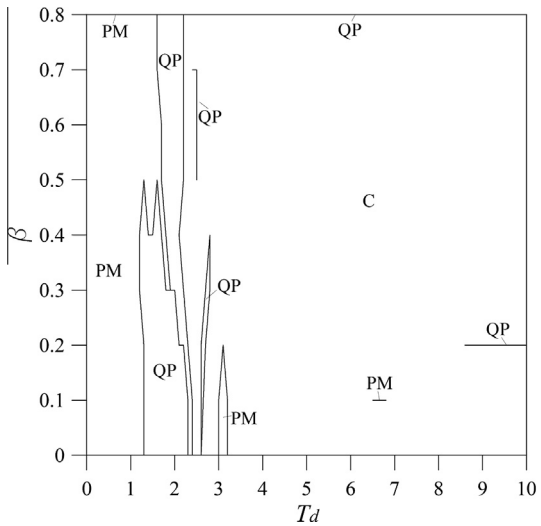

Fig. 16. Parameter domains (T_d, β) admitting periodic motion (PM), quasiperiodic motion (QP) and deterministic chaos (C), under the variation of μ, with $\delta_s = 1.0$ and $\omega_s = 0.5$. Other parameter values are: $s_0 = 1.0$, $\lambda = 1.5$, $\kappa = 2.0$ and $\gamma = 1.0$. Diagram is constructed for step size equal 0.1 for both T_d and β. For $\beta = 0.9$, velocity of the block becomes negative, meaning that block moves upwards which is neglected in our analysis.

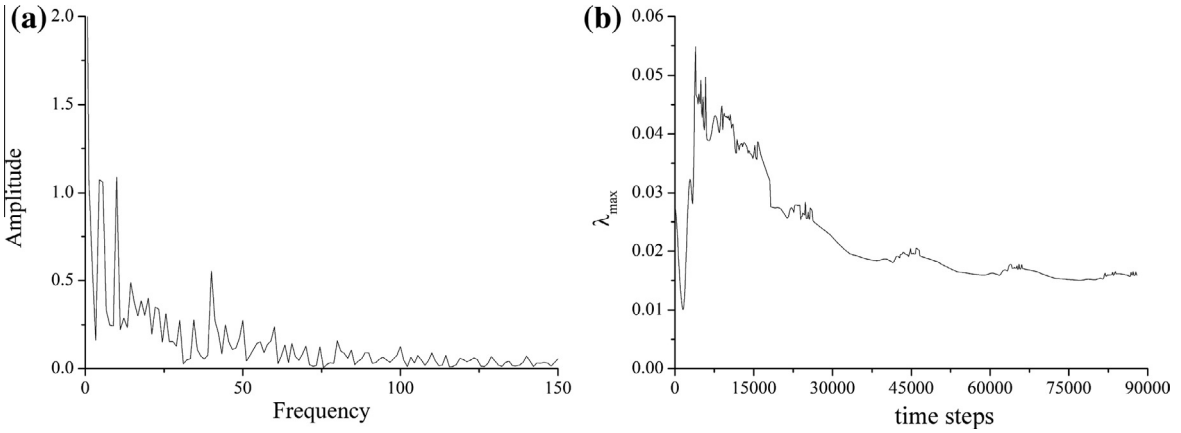

Fig. 17. (a) The broadband noise in the Fourier power spectrum indicates the chaotic behavior of the system for $T_d = 5$, $\beta = 0.3$; (b) maximal Lyapunov exponent converges well to $\lambda_{max} = 0.016$, indicating the presence of deterministic chaos. Other parameter values are identical to those in Fig. 16.

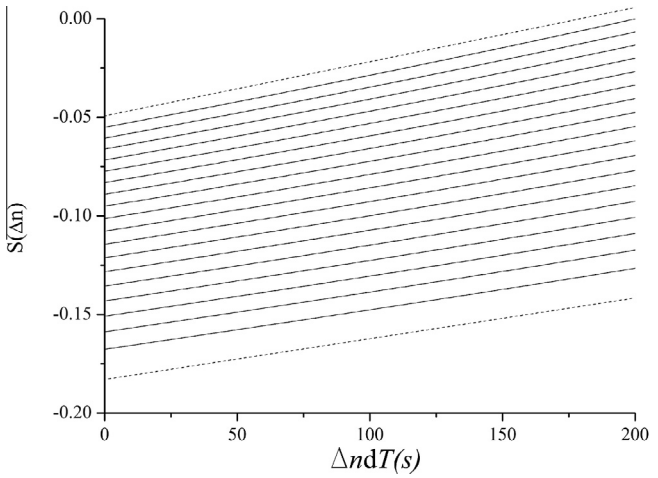

Fig. 18. Calculation of maximal Lyapunov exponent for the system (5) under the variation of μ, with $\delta_s = 1.0$ and $\omega_s = 0.5$. Other parameter values are: $T_d = 5$, $\beta = 0.3$, $s_0 = 1.0$, $\lambda = 1.5$, $\kappa = 2.0$ and $\gamma = 1.0$. The method of Rosenstein et al. [41], implies $\lambda_{max} \approx 0.012–0.016$. The results are determined for 100 reference points and neighboring distance $\varepsilon = 1–3$. The obtained value of maximal Lyapunov exponent is of the same order of magnitude, as in Fig. 17(b).

On the other hand, for $\beta > 1$, also by perturbing only the shear stress μ, velocity of the block takes negative values until $\omega_s = 4.9$, after which it becomes positive again and further increasing (Fig. 14). It has to be emphasized that in this case, similar to the previous one with time delay, system (12) is very stiff in numerical sense.

However, one could note that the observed dynamics is generated for the limit amplitude values ($\delta_s = s_0 = 1.0$), which are rarely observed in real conditions. In other words, it is highly unlikely to expect that the shear stress along the slip surface would change from maximum to zero value, since both field and laboratory tests indicate that even in the steady state, shear stress retains a certain minimum positive value. Hence, it is of special interest to investigate whether small parameter perturbations could lead to complex dynamics. Following this idea, additional analysis is conducted for all three dynamical regimes ($\beta < 1$, $\beta = 1$, $\beta > 1$), by decreasing oscillation amplitudes, while other parameter values are being held constant. For $\beta < 1$, variation of amplitude value does not render any new dynamics (it remains oscillatory). However, for $\beta = 1$, velocity of the block changes periodically for $\delta_s \leqslant 0.11$ (Fig. 15a). As for $\beta > 1$, velocity of the block rises exponentially for amplitude values $\delta_s \leqslant 0.22$ (Fig. 15b).

5. Co-effect of time delay and stress perturbation

In the final phase of the analysis, the periodic perturbation of parameter s_0 is assumed in system (5) with included time delay T_d, for $\delta_s = 1.0$ (limit amplitude value) and $\omega_s = 0.5$. In this case, attractors of the system (5) are shown in Fig. 16 for $\beta < 1$ and for T_d in range [0.1–10].

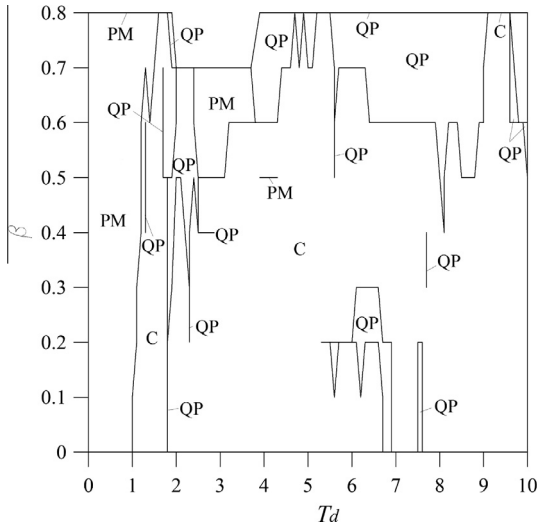

Fig. 19. Parameter domains (T_d, β) admitting periodic motion (PM), quasiperiodic motion (QP) and deterministic chaos (C), under the variation of μ, with $\delta_s = 0.5$ and $\omega_s = 0.5$. Other parameter values are: $s_0 = 1.0$, $\lambda = 1.5$, $\kappa = 2.0$ and $\gamma = 1.0$. Diagram is constructed for step size equal 0.1 for both T_d and β. For $\beta = 0.9$, velocity of the block becomes negative, meaning that block moves upwards which is neglected in our analysis.

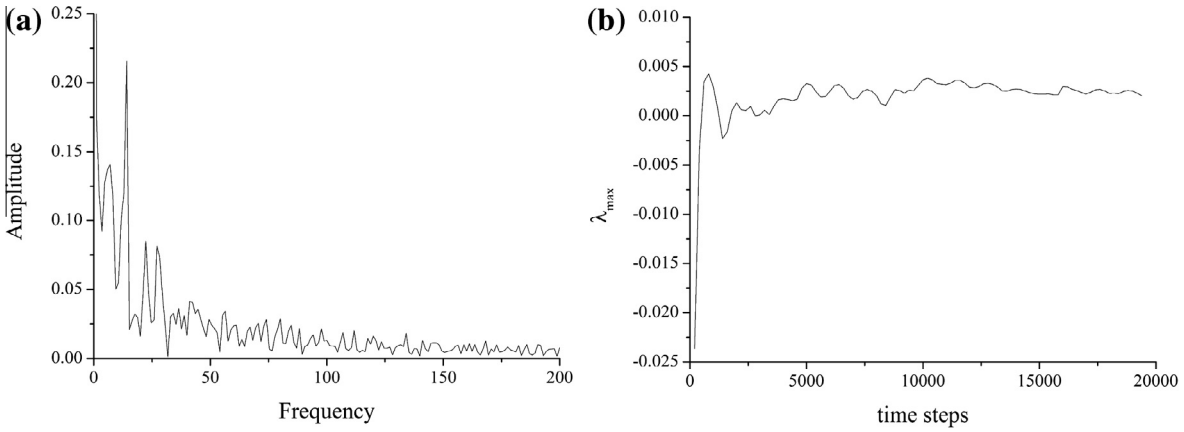

Fig. 20. (a) Continuous broadband noise in Fourier power spectrum confirms chaotic motion of block for $\beta = 1.1$, $T_d = 0.1$, $\delta_s = 0.15$ and $\omega_s = 0.5$; (b) maximal Lyapunov exponent converges well to positive value, $\lambda_{\max} = 0.002$. Other parameter values are: $s_0 = 1.0$, $\lambda = 1.5$, $\kappa = 2.0$ and $\gamma = 1.0$.

The onset of deterministic chaos is corroborated by broadband noise in power spectrum (Fig. 17a) and positive value of the largest Lyapunov exponent (Figs. 17b and 18).

It should be noted that the complex dynamics (Fig. 16) is observed for the limit amplitude value of initial stress oscillation ($\delta_s = 1.0$). The results of additional analysis, for $\beta < 1$ and for smaller amplitude values indicated even more complex behavior. Diagram in Fig. 19 is constructed for oscillation amplitude $\delta_s = 0.5$.

For $\beta = 1$ and for $\beta > 1$, and for the limit perturbation amplitudes ($\delta_s = 1.0$), block's velocity is changing periodically in negative domain, which is neglected in our analysis. However, if we assume smaller shear perturbation amplitudes, complex dynamical behavior emerges. For $\beta = 1$, if we take that $\delta_s = 0.06$ (as in Fig. 15), while the other parameter values are as in Fig. 19, the introduction of time delay T_d slows down the block, and for $T_d = 0.4$, the block's velocity becomes negative. Similar behavior is observed for other amplitude values in the range $[0, 1]$. As for $\beta > 1$, systematic exploration reveals the following dynamics. For $T_d = 0.1$, system (5) exhibits chaotic dynamics, if the perturbation amplitude is $\delta_s \leqslant 0.18$, while for $\delta_s > 0.18$, as already stated, block's velocity is changing periodically in negative domain. Deterministic chaos is further corroborated by broadband noise in Fourier power spectrum and by positive value of maximal Lyapunov exponent (Figs. 20 and 21).

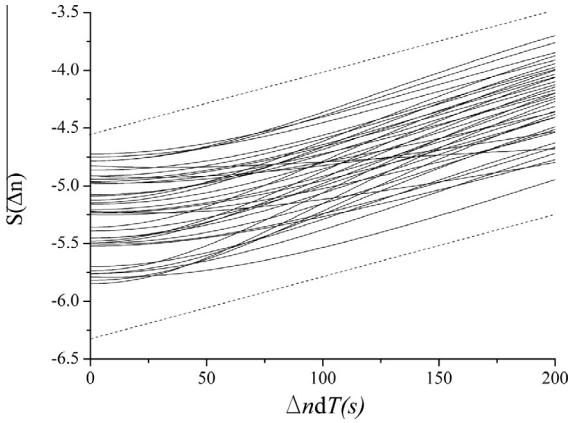

Fig. 21. Calculation of maximal Lyapunov exponent for the system (5) under the variation of μ, with $\delta_s = 0.15$ and $\omega_s = 0.5$. Other parameter values are: $\beta = 1.1$, $T_d = 0.1$, $s_0 = 1.0$, $\lambda = 1.5$, $\kappa = 2.0$ and $\gamma = 1.0$. The method of Rosenstein et al. [41], implies $\lambda_{max} \approx 0.005$. The results are determined for 1000 reference points and neighboring distance $\varepsilon = 0.005–0.015$. The obtained value of maximal Lyapunov exponent is of the same order of magnitude, as in Fig. 20(b).

6. Discussion and conclusion

In present paper, we examined the dynamics of the block along the inclined slope, under the variation of two parameters: time delay T_d and initial shear stress s_0. We assume that this model phenomenologically describes sliding along the infinite slope. Parameter T_d mimics the memory effect of the sliding surface, and it is usually interpreted as a function of history of sliding. Also, it could be related to the initial retarded period of the frictional healing during quasistationary contact, which is a feature commonly observed in dynamics of earthquake faults [6,26]. In the same time, this parameter serves as a replacement for the second state variable θ, bringing closer in that way the effects of one-state and two-state Dieterich–Ruina friction law. On the other hand, external dynamic effect of long lasting shear waves or traffic vibrations is modeled by periodic perturbations of initial shear stress μ. It has to emphasized that sinusoidal oscillations represent idealistic case of perturbations, which rarely occur in natural conditions. However, as already stated in the introductory part, we believe they are of interest because of their simple shape, and because a real wave pattern results in a superposition of such periodic waves. Also, some long-lasting earthquakes could generate seismic waves of such simple shape [28], or they could occur as a product of some artificial source, e.g. mining vibrations. They also represent the basis for more complex periodic perturbations represented by a sine wave scaled by a Gaussian pulse [42].

In the first phase of the research, each parameter is varied separately, in order to estimate their independent effect on dynamics of motion. The variation of these parameters generate various types of dynamics depending on parameter β, which is confirmed by previous research [16,17] as a control parameter that primarily defines the stability of the system. For $\beta < 1$, the change of parameter T_d renders rich dynamical behavior, with transition from equilibrium state through periodic and quasiperiodic motion to deterministic chaos (Fig. 2). This type of dynamics significantly differs from the original case without T_d, when the block is in the creeping phase, with the equilibrium point as an improper node [16]. It has to be emphasized that the dynamics of the model (5) with the introduced time delay was examined in two ways: using the standard local bifurcation analysis and numerical approach. Even though the results in both cases are qualitatively similar and indicate the existence of complex dynamics, numerical approach showed additional small areas of complex behavior that were not captured by local bifurcation analysis. This type of behavior could be explained by the effect of global bifurcations, which were not analyzed in present paper. However, by introducing the oscillatory character of the shear stress μ without the influence of time delay, while the other parameters are held constant for the initially creeping slope, the analysis shows that block exhibits only oscillatory behavior. For $\beta = 1$, the introduction of time delay has an opposite effect – it suppresses the motion, by slowing down the block and generating transition to equilibrium state (Fig. 9). This is contrast to the original model, where only the constant positive velocity of the block is observed, with equilibrium point as a neutrally stable one. On the other hand, perturbation of stress parameter μ for $\beta = 1$ generates negative velocity of the block, which is the case that is not observed in nature. This type of dynamics occurs for limit amplitude values ($\delta_s = s_0 = 1.0$). By decreasing the amplitude values, it is observed that for $\delta_s \leqslant 0.11$, velocity of the block changes periodically, simultaneously decreasing with time (Fig. 15a). For $\beta > 1$ and with introduced T_d, system (5) becomes very stiff in numerical sense, so the analysis was done only for $\beta = 1.1$, when the chaotic behavior is observed (Figs. 10 and 11). On the other hand, perturbation of μ for $\beta > 1$ (and for limit amplitude value) renders the physically acceptable behavior only for high frequencies ($\omega_s > 4.9$), when the oscillatory motion of the block with increasing amplitude occurs (Fig. 14). By decreasing the amplitude value, for $\delta_s \leqslant 0.22$ velocity of the block rises exponentially (Fig. 14b).

In the second phase of the research, combined effect of both parameters is analyzed for the limit amplitude values ($\delta_s = s_0 = 1.0$). For $\beta < 1$, complex dynamic behavior is also observed, with transition from periodic and quasiperiodic motion to deterministic chaos (Fig. 16). As it is obvious, dynamics of the model is more complex in this case, meaning that the onset

of chaos is observed for much lower values ($T_d = 2.3$, $\beta = 0.5$) in comparison to the previous one, when only parameter T_d is varied ($T_d = 6.7$, $\beta = 0.1$). Moreover, if we assume initial shear oscillations of smaller amplitudes ($\delta_s = s_0 = 0.5$) more complex behavior occurs (Fig. 19). In real conditions, it means that external triggering effect of earthquake or some other source of vibrations of any amplitude could easily generate instability and occurrence of sliding along the slope. For $\beta = 1$ and for $\beta > 1$, the velocity of the block is negative, which does not correspond to real conditions on an inclined slope. However, if we assume smaller perturbation amplitude values, complex dynamical behavior emerges. For $\beta = 1$ and for the amplitude values in the range [0,1] the introduction of time delay T_d slows down the block, and for $T_d = 0.4$, block takes negative velocity. As for $\beta > 1$, the introduction of time delay T_d (while in the same time initial stress is periodically perturbed), systematic exploration reveals the following dynamics. For $T_d = 0.1$, system (5) exhibits chaotic dynamics, if the perturbation amplitude is $\delta_s \leqslant 0.18$ (Fig. 20). For $T_d > 0.1$ and for $\delta_s < 0.18$, system (5) becomes extremely stiff in numerical sense, meaning that very small iteration steps are required in order to conduct numerical integration.

The performed analysis showed that the most complex dynamics of motion along the slope is observed for $\beta < 1$, which corresponds well to the experimental results of Skempton [13]. Apparently, this velocity-strengthening behavior is observed in ring shear laboratory tests for friction stress variations with slip rate changes, for Kalabagh Dam clay and siltstone with low clay fraction. The results of these experiments indicated that the decrease of frictional stress with the ongoing slip (B) was lower in comparison to the increase of shear stress along the slip surface (A) when the sudden increase in velocity occurs ($B < A$).

In comparison to the original model (3), our analysis shows that the instability of motion along the slope could occur even for $\beta < 1$ with introduced time delay, while Chau [16] observed the appearance of instable motion only for $\beta > 1$, which is, as already stated, the case that is not detected in laboratory conditions [13]. In present analysis, complex dynamics in velocity-weakening regime occurs only for small values of time delay ($T_d = 0.1$) and relatively small perturbation amplitudes ($\delta_s \leqslant 0.18$).

We have to emphasize that the idea of a chaotic landslide dynamics has already been suggested in [43], where it is shown that chaos appears in the evolutionary process of a slope. Moreover, Qin et al. [44] reported that slope body evolves from a chaotic through periodic and deterministic motion.

Interesting result is certainly the dual effect of time delay T_d on the motion of the block (meaning that it renders the complex dynamics, and, in the same time, stabilizes the motion of the block) depending on the value of the control parameter β. As it was shown, for $\beta < 1$, introduction and variation of T_d generates complex dynamics, with the complete Ruelle–Takens–Newhouse route to chaos. On the other side, for $\beta = 1$, time delay has opposite effect, rendering the transition to equilibrium state.

Acknowledgments

This research has been supported by the Ministry of Education, Science and Technological development of the Republic of Serbia, Contracts No. 176016, 171015 and 171017.

References

[1] Helmstetter A, Sornette D, Grasso J-R, Andersen JV, Gluzman S, Pisarenko V. Slider-block friction model for landslides: application to Vaiont and La Clapiere landslides. J Geophys Res Sol Ea 2004;109:B02409.
[2] Skempton AW. Long-term stability of clay slopes. Geotechnique 1964;14:77–102.
[3] Wang J. Comparisons of limit analysis solutions and random search solutions on slope critical slip surface. Commun Nonlinear Sci 1998;3:66–71.
[4] Labuz J, Zang A. Mohr–Coulomb failure criterion. Rock Mech Rock Eng 2012;45:975–9.
[5] Gomberg J, Beeler N, Blanpied M. On rate-state and Coulomb failure models. J Geophys Res 2000;105:7857–71.
[6] Marone C. The effect of loading rate on static friction and the rate of fault healing during the earthquake cycle. Nature 1998;391:69–72.
[7] Scholz C. Earthquakes and friction laws. Nature 1998;391:37–42.
[8] Dieterich JH. Modeling of rock friction – 1. Experimental results and constitutive equations. J Geophys Res 1979;84:2161–8.
[9] Ruina A. Slip instability and state variable friction laws. J Geophys Res 1983;88:359–70.
[10] Rice JR, Ruina A. Stability of steady frictional slipping. Trans Am Soc Mech Eng 1983;50:343–9.
[11] Gu J-C, Rice JR, Ruina AL, Tse ST. Slip motion and instability of a single degree of freedom elastic system with rate and state dependent friction. J Mech Phys Solids 1984;32:167–96.
[12] Tullis TE, Weeks JD. Constitutive behavior and stability of frictional sliding of granite. Pure Appl Geophys 1986;124:383–414.
[13] Skempton AW. Residual strength of clays in landslides, folded strata and the laboratory. Geotechnique 1985;35:3–18.
[14] Carlson JM, Langer JS. Mechanical model of an earthquake fault. Phys Rev A 1989;40:6470–84.
[15] Erickson B, Birnir B, Lavallee D. A model for aperiodicity in earthquakes. Nonlinear Process Geophys 2008;15:1–12.
[16] Chau KT. Landslides modeled as bifurcations of creeping slopes with nonlinear friction law. Int J Solids Struct 1995;32:3451–64.
[17] Chau KT. Onset of natural terrain landslides modeled by linear stability analysis of creeping slopes with a two-state variable friction law. Int J Numer Anal Methods 1999;23:1835–55.
[18] Weeks JD, Tullis TE. Frictional sliding of dolomite: a variation in constitutive behavior. J Geophys Res 1985;90:7821–6.
[19] Crosta G, Imposimato S, Roddeman D. Numerical modelling of large landslides stability and runout. Nat Hazards Earth Syst Sci 2003:523–38.
[20] Martelloni G, Bagnoli F, Massaro E. A computational toy model for shallow landslides: molecular dynamics approach. Commun Nonlinear Sci 2013;18:2479–92.
[21] Eisbacher GH. Cliff collapse and rock avalanches in the Mackenzie Mountains, Northwestern Canada. Can Geotech J 1979;16:309–34.
[22] Davis RO, Smith NR, Salt G. Pore fluid frictional heating and stability of creeping landslides. Int J Numer Anal Methods 1990;14:427–43.
[23] Durville JL. Study of mechanisms and modeling of large slope movements. Bull Eng Geol Environ 1992;45:25–42.
[24] Savage WZ, Chleborad AF. A model for creeping flow in landslides. Bull Eng Geol Environ 1982;19:333–8.
[25] Davis RO, Desai CS, Smith NR. Stability of motion of translational landslides. J Geotech Eng ASCE 1993;119:420–32.
[26] Kostić S, Franović I, Todorović K, Vasović N. Friction memory effect in complex dynamics of earthquake model. Nonlinear Dyn 2013;73:1933–43.

[27] Fleming RW, Johnson AM. Structures associated with strike-slip faults that bound landslide elements. Eng Geol 1989;27:39–114.
[28] Gomberg J, Bodin P, Savage W, Jackson ME. Landslide faults and tectonic faults, analogs? – The slumgullion earthflow, Colorado. Geology 1995;23:41–4.
[29] Peng Z, Gomberg J. An integrated perspective of the continuum between earthquakes and slow-slip phenomena. Nat Geosci 2010;3:599–607.
[30] Schreyer HL. Inverse solutions for one-dimensional seismic waves in elastic, inhomogeneous media. J Appl Mech 1997;44:469–74.
[31] Burić N, Vasović N. A simple model of the chaotic immune response. Chaos Solitons Fractals 1999;10:1185–92.
[32] C. Scholz, The mechanics of earthquakes and faulting, Cambridge University Press, United Kingdom; 2002. p. 471.
[33] Clancy I, Corcoran D. State-variable friction for the Burridge–Knopoff model. Phys Rev E 2009;80:016113.
[34] Y. Pomeau, M. Le Berre, Critical speed-up vs critical slow-down: a new kind of relaxation oscillation with application to stick-slip phenomena, arXiv: 1107.3331v1 (2011) pp. 1–8.
[35] Belair J, Campbell SA. Stability and bifurcations of equilibria in a multiple delayed differential equation. SIAM J Appl Math 1994;54:1402–24.
[36] Wiggins S. Introduction to applied nonlinear dynamical systems and chaos. New York: Springer; 2003.
[37] Kuznetsov YA. Elements of the applied bifurcation theory. New York: Springer-Verlag; 2004.
[38] Ruelle D, Takens F. On the nature of turbulence. Commun Math Phys 1971;20:167–72.
[39] Newhouse S, Ruelle D, Takens F. Occurrence of strange axiom-A attractors near quasiperiodic flow on 7, m > 3. Commun Math Phys 1978;64:35–44.
[40] Wolf A, Swift J, Swinney H, Vastano J. Determining Lyapunov exponents from a time series. Physica D 1985;16:285–317.
[41] Rosenstein MT, Collins JJ, De Luca CJ. A practical method for calculating largest Lyapunov exponents from small data sets. Physica D 1993;65:117–34.
[42] Gomberg J, Blanpied M, Beeler N. Transient triggering of near and distant earthquakes. Bull. Seismolog Soc Am 1997;87:294–309.
[43] Qin S, Jiao JJ, Wang S, Long H. A nonlinear catastrophe model of instability of planar-slip slope and chaotic dynamical mechanisms of its evolutionary process. Int J Solids Struct 2001;38:8093–109.
[44] Qin S, Jiao JJ, Wang S. A nonlinear dynamical model of landslide evolution. Geomorphology 2002;43:77–85.